

## 13.2: A Floating-Gate OTFT-Driven AMOLED Pixel Circuit for Variation and Degradation Compensation in Large-Sized Flexible Displays

Tsung-Ching Huang<sup>1</sup>, Koichi Ishida<sup>1</sup>, Tsuyoshi Sekitani<sup>2</sup>, Makoto Takamiya<sup>1</sup>,  
Takao Someya<sup>2</sup>, and Takayasu Sakurai<sup>1</sup>

<sup>1</sup>Institute of Industrial Science, University of Tokyo, Japan

<sup>2</sup>Department of Electrical Engineering, University of Tokyo, Japan

### Abstract

For the first time, we demonstrate an AMOLED pixel circuit on a 13- $\mu\text{m}$  thick plastic film that applies floating-gate OTFTs (FG-OTFTs) to compensate for OTFT driving current variations and OLED efficiency degradations. By programming  $V_{\text{TH}}$  of the FG-OTFTs, we can realize less than 5% spatial non-uniformity and 85% power reduction compared with voltage-programming.

### 1. Introduction

AMOLED displays have attracted much attention recently because of their excellent image quality and wide viewing angle [1-2]. Organic TFT (OTFT) is considered as a strong candidate for pixel circuits of large-size flexible displays, because of its mechanical flexibility and compatibility with the low-cost printing process at room temperature [3-4]. OTFT-driven AMOLED displays, therefore, are a promising solution for realizing next-generation large-size, light-weight, and mechanically robust flexible displays. To print a large number of OTFTs on large-area flexible substrates with high-uniformity, however, is very challenging and has become the major bottleneck for realizing large-size OTFT-driven AMOLED flexible displays.

In this paper, for the first time, we demonstrate a FG-OTFT-driven AMOLED pixel circuit for flexible displays as shown in Fig. 1. The pixel circuit enables electrical feedback to tune  $V_{\text{TH}}$  of the FG-OTFT for compensating OTFT variations and OLED efficiency degradations. Unlike voltage-programming or current-programming [5-6] that require  $V_{\text{TH}}$  compensation in every frame time, the programmed  $V_{\text{TH}}$  in our FG-OTFTs can retain for tens of hours and no further  $V_{\text{TH}}$  programming is needed within the retention time. The proposed work, therefore, has several key advantages over conventional methods including: 1) low power-consumption by eliminating  $V_{\text{TH}}$  compensation cycle in the frame time, 2) compensation for both OTFT non-uniformity and OLED

efficiency degradations, and 3) higher aperture ratio and yield because of reduced transistor counts (3T-1C).

#### 1.1. Floating-Gate Organic TFTs

Fig. 2 shows the cross-section of a 20V FG-OTFT. The channel length  $L$  is 20  $\mu\text{m}$  and the organic semiconductor in our p-type FG-OTFT is DNTT [7] with carrier mobility of 0.7  $\text{cm}^2/\text{Vs}$ . While the 20V FG-OTFT can work as a normal OTFT with -20V gate-voltage  $V_{\text{GS}}$ , its  $V_{\text{TH}}$  can be adjusted by applying high-voltage electrical stresses to the gate terminal. As shown in Fig. 3, when the source and drain terminals of a FG-OTFT are grounded and no drain-source current is conducting, the electron holes can be injected from the Parylene gate insulator to the Au floating gate by applying a pulsed high voltage such as -60V to its gate terminal. These injected holes can be kept in the Au floating-gate and reduce electrical field from the gate voltage to the organic semiconductor. The effective  $V_{\text{TH}}$  of the FG-OTFT is therefore increased until the injected electron holes completely escape. More details about our FG-OTFTs can be found elsewhere in [8].

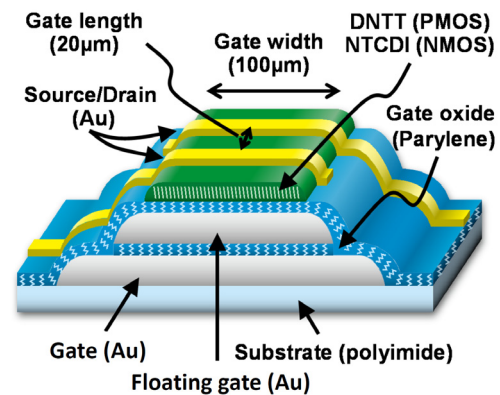


Figure 2: Cross section of a 20V FG-OTFT.

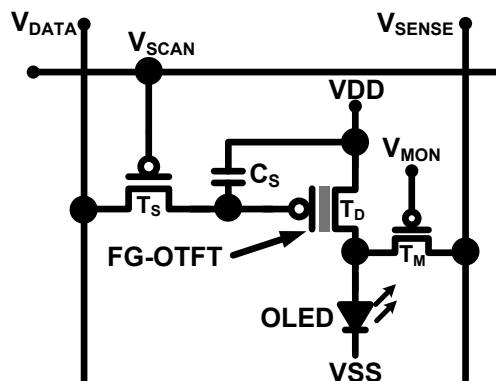


Figure 1: Proposed AMOLED 3T-1C pixel-circuit.

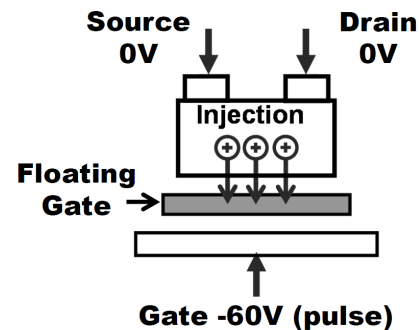


Figure 3: Working principle of a FG-OTFT.

1.2. Pixel Structure

Fig. 4 shows typical voltages of  $V_{DATA}$ ,  $V_{SCAN}$ ,  $V_{MON}$ , and  $V_{SENSE}$  in Fig. 1 for monitoring FG-OTFT non-uniformity and OLED efficiency degradations, as well as programming  $V_{TH}$  of the FG-OTFT. In order to monitor the driving current of  $T_D$  as shown in Fig. 4 without being affected by  $V_{TH}$  variations of  $T_M$ ,  $V_{CAL}$  was set sufficiently close to  $V_{TH}$  of  $T_D$  while  $V_G$  of  $T_M$  was set to a higher voltage such as -40V to keep the on-resistance of  $T_D$  much higher than that of  $T_M$  as shown in Fig. 4(a). Fig. 5 shows SPICE-simulated  $T_D$  current measurement errors due to  $V_{TH}$  variations of  $T_M$ . We can find that the current measurement error can be minimized to less than 5% even under 20%  $V_{TH}$  variations of  $T_M$  because the measured current was mainly determined by  $T_D$  in the saturation region rather than  $T_M$  in the linear region. Fig. 4(b) shows the configuration of monitoring OLED efficiency degradation.  $T_D$  was switched off by setting  $V_{GS}$  of  $T_D$  to be 10V and  $V_{SENSE}$  was set close to  $V_{TH}$  of OLED (~6V) to minimize  $V_{DS}$  of  $T_M$  for reducing current measurement errors. The OLED efficiency degradation can then be estimated by measuring  $V_{TH}$  of OLED at a given current.  $V_{DATA}$  and  $V_{TH}$  of  $T_D$  can be adjusted accordingly to compensate for OLED efficiency degradations.

Fig. 4(c) shows the configuration of  $V_{TH}$  programming for  $T_D$ . A pulsed electrical stress -60V was applied to the gate terminal of  $T_D$  through  $T_S$ .  $V_D$  and  $V_S$  of  $T_D$  were both set to 0V during  $V_{TH}$

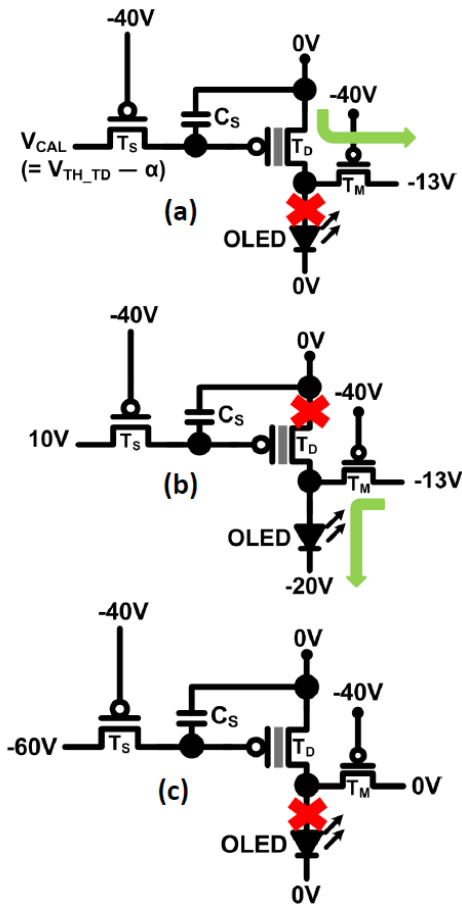


Figure 4: (a) Monitoring FG-OTFT driving current, (b) monitoring OLED efficiency degradations, and (c) applying electrical stress for  $V_{TH}$  programming.  $W_{TD} = 6$  cm,  $W_{TM} = W_{TS} = 0.3$  cm, and  $C_S = 2$  pF in our pixels.

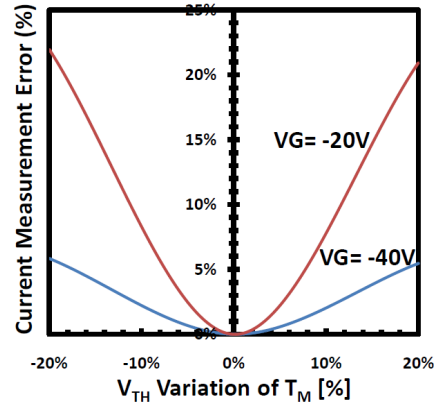


Figure 5: SPICE-simulated current measurement error due to  $V_{TH}$  variations of  $T_M$ .  $V_G$  is the gate voltage of  $T_M$ .

programming such that no current is conducting through  $T_D$ . The measurement results and the scheme of  $V_{TH}$  programming for minimizing non-uniformity and power consumption are followed.

2. Measurement Results

2.1.  $V_{TH}$  Programming

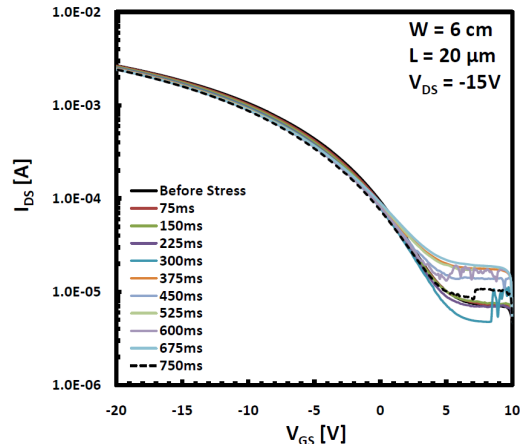


Figure 6:  $V_{TH}$  programming process for a FG-OTFT with (-60V, 75ms) step size of electrical stress.

To perform quantitative analysis of  $V_{TH}$  programming, we applied a digital control method by fixing the stress voltage  $V_{STRESS}$  to -60V and varying the number of stress pulses and the pulse-width for  $V_{TH}$  control. Fig. 6 shows the measurement results of the FG-OTFT driving currents during  $V_{TH}$  programming process with (-60V, 75ms) stress conditions. The device size of the FG-OTFT was made large to provide sufficient driving currents for our OLEDs to achieve peak brightness greater than 200 cd/m<sup>2</sup>. From Fig. 6 we can observe that  $V_{TH}$  increases with the stress time due to injected electron holes in the floating-gate. The programmed  $V_{TH}$  can retain for tens of hours until full recovery to its original  $V_{TH}$ . Since  $V_{DS}$  of the FG-OTFT was kept to 0V during  $V_{TH}$  programming, the measured drain-source current  $I_{DS}$  of  $T_D$  during  $V_{TH}$  programming was lower than 1nA, which was six orders or less than its saturation current and therefore consumed negligible power compared with OLED driving.

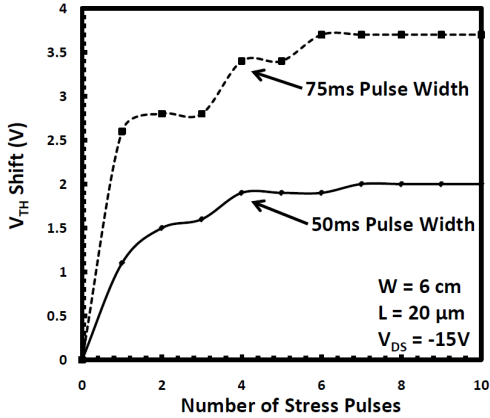


Figure 7: The relationship between  $V_{TH}$  shifts and pulse.

Fig. 7 shows the relationship among  $\Delta V_{TH}$ , stress pulse width, and stress time with  $-60V$  stress voltage. Here  $V_{TH}$  is defined as  $(W/L \times 50nA)$  using the constant current method, where  $W$  is the channel width and  $L$  is the channel length. We can learn from Fig. 7 that larger stress voltage  $V_{STRESS}$  and longer stress time  $T_{STRESS}$  can result in greater  $V_{TH}$  shifts. The measured  $\Delta V_{TH}$  can be fitted to Eqn.1 where  $\alpha$  and  $\beta$  are fitting parameters.

$$\Delta V_{TH} = V_{Stress}^{\alpha} \log_{\beta}(T_{Stress}) \quad (1)$$

### 2.2. Variation Compensation for Pixel Circuit

To demonstrate variation compensation by  $V_{TH}$  programming, we prepared six identical FG-OTFT-driven AMOLED pixels in a  $2 \times 3$  array on the same polyimide plastic film. In order to illustrate the effects of electrical stress, Fig. 8 shows  $I_{DRIVE}-V_{DATA}$  plots of two AMOLED pixels and the inset shows the variations before and after applying electrical stress. We can see that the driving current difference was larger than 15% initially and this difference was minimized to less than 2% after applying total 525ms stress with  $(-60V, 75ms)$  stress pulses. Note that the stress conditions can be further optimized to meet the requirements of  $V_{TH}$  control resolution, total stress time, and required spatial uniformity. The  $V_{TH}$  programming scheme for variations and degradations compensation is illustrated using a flowchart as shown in Fig. 9.  $V_{TH}$  monitoring and electrical stress are provided through external

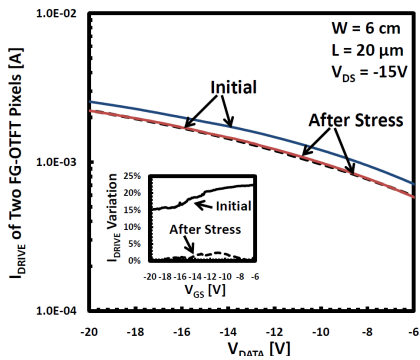


Figure 8: Variation compensations for two neighboring AMOLED pixels (blue and red solid-lines). Black broken-line shows the after-stress  $I_{DRIVE}$  while blue solid-line shows the before-stress  $I_{DRIVE}$  of the identical AMOLED pixel.

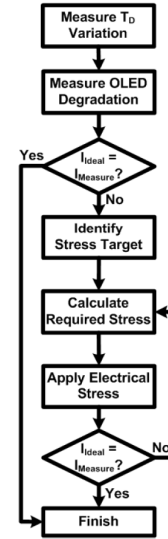


Figure 9: Flowchart of measuring and compensating OTFT variations and OLED degradations.

circuitry.  $T_D$  in Fig. 9 represents the FG-OTFT-based OLED driver as shown in Fig. 4. Fig. 10 shows the compensation results for all six AMOLED pixels. The broken lines represent the initial driving currents provided by FG-OTFTs before-stress while solid lines are driving currents after  $V_{TH}$  programming, which scheme is illustrated in Fig. 9. The inset of Fig. 10 shows that the driving current variation, represented by standard deviations, was reduced from 14% to less than 5% after  $V_{TH}$  programming. Although here only shows the results for total six pixels, the  $V_{TH}$  programming scheme can be easily applied to all AMOLED pixels in flexible displays for minimizing spatial non-uniformity.

The OLED efficiency degradations can also be compensated by monitoring  $V_{TH}$  of OLEDs at known input currents through  $T_M$  as shown in Fig. 4(b), which can be used to indicate the degree of OLED efficiency degradations for  $T_D$  current compensations.

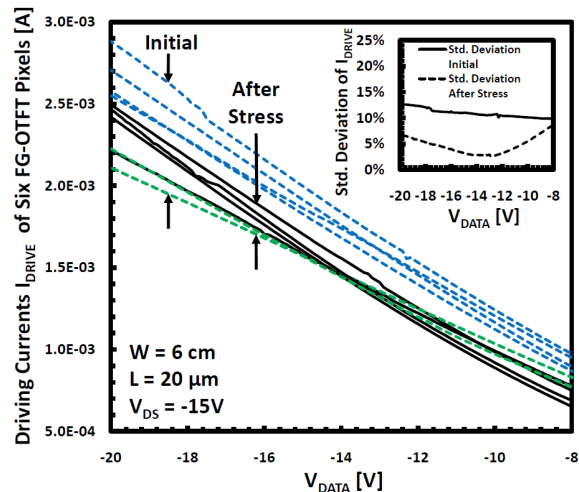
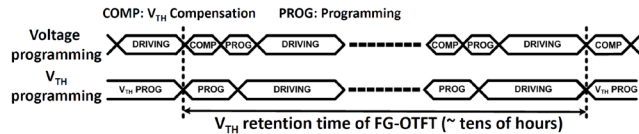
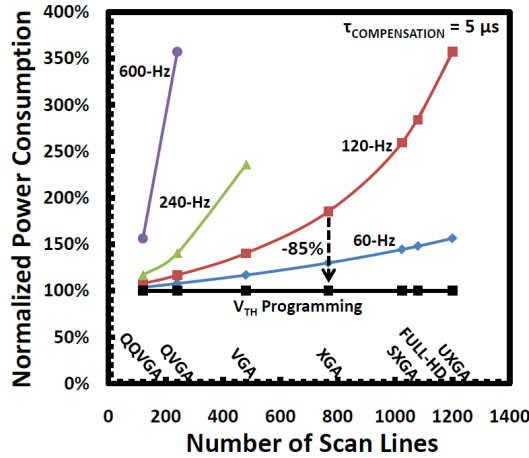


Figure 10: Driving currents  $I_{DRIVE}$  of total six pixels before-stress (broken-line) and after-stress (solid-line). The inset shows the standard deviations of  $I_{DRIVE}$ . Green broken lines show no-need-to-stress pixels due to initially lower driving currents.



**Figure 11: Timing diagram for conventional voltage-programming and proposed  $V_{TH}$  programming schemes.  $V_{TH}$  programming process can retain  $V_{TH}$  for tens of hours.**



**Figure 12: Normalized power consumption  $P_{PIXEL}$  of an AMOLED pixel under different display resolutions and refresh rates using voltage-programming scheme. Proposed  $V_{TH}$  programming is used as the reference for comparisons.**

### 2.3. Power Reduction

In addition to variation and degradation compensation, the proposed FG-OTFT pixel circuit also lowers the pixel power consumption  $P_{PIXEL}$  because of eliminating the  $V_{TH}$  compensation cycle in the frame time  $\tau_{FRAME}$  ( $\tau_F$ ). For conventional compensation schemes such as voltage-programming,  $V_{TH}$  of the driving TFT is generated and stored in a capacitor that needs to be updated every frame time. In order to ensure that the stored  $V_{TH}$  is equal or close enough to the real  $V_{TH}$ , the required compensation time  $\tau_{COMPENSATION}$  ( $\tau_C$ ) should be longer than tens of micro-second ( $\mu s$ ) [9]. Since  $\tau_C$  reduces the driving time  $\tau_{DRIVING}$  ( $\tau_D$ ) as illustrated in Eqn. 2 for a given  $\tau_F$  and the compensation power  $P_{COMPENSATION}$  ( $P_C$ ) does not directly contribute to driving the OLED, the required  $P_{PIXEL}$  for the voltage-programming scheme within the reduced  $\tau_D$  in order to achieve the same peak brightness as the proposed  $V_{TH}$  programming scheme will therefore increase significantly. Fig. 11 shows the timing diagram and Fig. 12 shows the normalized pixel power consumption  $P_{PIXEL}$  for both voltage-programming and  $V_{TH}$  programming schemes. Note that  $P_{PIXEL}$  in Fig. 12 is calculated by assuming  $\tau_C$  equal to 5  $\mu s$  and the same average OLED driving currents  $I_{OLED}$  under the same  $\tau_F$  for both cases. While the proposed  $V_{TH}$  programming scheme using FG-OTFTs does not require the  $V_{TH}$  compensation cycle and consumes negligible power during the  $V_{TH}$  programming process, the voltage-programming scheme requires 85% power overhead if driven at the XGA resolution with 120-Hz refresh rate. Higher resolutions and refresh rates, as well as longer  $\tau_C$ , will inevitably increase the pixel power consumption due to the reduced  $\tau_D$ . Note that for high refresh rates such as 240-Hz and 600-Hz, higher

resolutions than VGA mode are unable to achieve in the voltage-programming scheme since  $\tau_F$  will be less than 5  $\mu s$  ( $=\tau_C$ ).

$$P_{PIXEL} = P_{COMPENSATION} + P_{PROGRAMMING} + P_{DRIVING} \quad (2)$$

$$\tau_{DRIVING} = \tau_{FRAME} - \tau_{COMPENSATION} - \tau_{PROGRAMMING}$$

## 3. Conclusion

In this paper, for the first time, we demonstrate a FG-OTFT driven AMOLED pixel circuit on a 13- $\mu m$  thick polyimide plastic film for compensating OTFT process variations and OLED efficiency degradations. The photo of the proposed FG-OTFT pixel-circuit is shown in Fig. 13. In our test sample, we prepared six identical pixels allocated in a 2x3 array. After applying the electrical stress to the driving FG-OTFTs, the overall spacial non-uniformity of the driving FG-OTFTs was minimized from 14% to be less than 5%. Compared with the conventional voltage-programming compensation scheme, the pixel power consumption can be reduced by 85% for the XGA resolution at 120-Hz refresh rate.

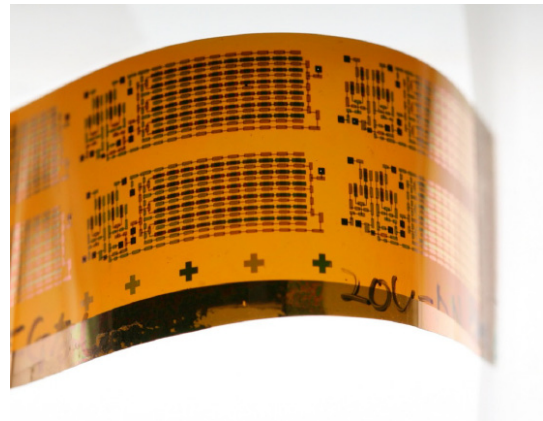


**Figure 13: Photo of the FG-OTFT-driven AMOLED pixels. The pixel size is 20.8 mm x 6.6 mm and substrate thickness is 13  $\mu m$ .**

## 4. Acknowledgements

We will like to thank for Japan Science and Technology Agency (JST) / Core Research for Evolutional Science and Technology (CREST) for financial supports.

## 5. References

- [1] D.-U. Jin et al, SID'09 DIGEST, pp. 983 (2009)
- [2] S. Okutani et al, SID'07 DIGEST, pp. 173 (2007)
- [3] M. Katsuhara et al, SID'09 DIGEST, pp. 656 (2009)
- [4] K. Nomoto, SID'10 DIGEST, pp. 1155 (2010)
- [5] A. Nathan et al, IEEE JDT'05, vol.1, iss. 2, pp. 267 (2005)
- [6] R. Stewart, SID'10 DIGEST, pp. 790 (2010)
- [7] dinaphtho[2,3-b:2',3'-f] thieno [3,2-b] thiophene (DNTT) T. Yamamoto, K. Takimiya, J. Am. Chem. Soc. 2007, 129, 2224.
- [8] T. Sekitani et al, Science 326, pp.1516 (2009)
- [9] G.R. Chaji et al, IEEE JDT'08, vol.4, iss. 2, pp. 233 (2008)